View Online / Journal Homepage
Dynamic Article Links

Catalysis
Science & Technology

Cite this: DOI: 10.1039/c2cy20383a

www.rsc.org/catalysis

PAPER

Substitution of WO_3 in $V_2O_5/WO_3–TiO_2$ by Fe_2O_3 for selective catalytic reduction of NO with NH_3

Shijian Yang,[abc] Chizhong Wang,[b] Lei Ma,[b] Yue Peng,[b] Zan Qu,[c] Naiqiang Yan,[c] Jinghuan Chen,[b] Huazhen Chang[b] and Junhua Li*[b]

Received 6th June 2012, Accepted 31st August 2012
DOI: 10.1039/c2cy20383a

To improve N_2 selectivity and lower the cost, WO_3 in $V_2O_5/WO_3–TiO_2$ was substituted by a low cost composition Fe_2O_3 for selective catalytic reduction (SCR) of NO with NH_3. The SCR reaction over $V_2O_5/Fe_2O_3–TiO_2$ mainly followed the Eley–Rideal mechanism (*i.e.* the reaction between activated ammonia species and gaseous NO). There were two active components on $V_2O_5/WO_3–TiO_2$ for the activation of adsorbed NH_3 (*i.e.* V^{5+} and Fe^{3+}). The acid sites on $V_2O_5/Fe_2O_3–TiO_2$ mainly resulted from the support $Fe_2O_3–TiO_2$, so the adsorbed NH_3 preferred to be activated by Fe^{3+} rather than by V^{5+}. V^{5+} on $V_2O_5/Fe_2O_3–TiO_2$ could accelerate the regeneration of Fe^{3+} on $Fe_2O_3–TiO_2$ due to the rapid electron transfer between V^{5+} and Fe^{2+} on the surface, so the activation of adsorbed NH_3 by Fe^{3+} was promoted. As some NH_3 adsorbed on $V_2O_5/Fe_2O_3–TiO_2$ was not activated by Fe^{3+}, the inactivated NH_3 could then be activated by V^{5+} on the surface. As a result, 2% $V_2O_5/Fe_2O_3–TiO_2$ showed excellent SCR activity, N_2 selectivity and H_2O/SO_2 durability at 300–450 °C. Furthermore, the emission of 2% $V_2O_5/Fe_2O_3–TiO_2$ to the fly ash can be prevented by an external magnetic field due to its inherent magnetization. Therefore, 2% $V_2O_5/Fe_2O_3–TiO_2$ could be a promising low-cost catalyst in NO emission control.

1. Introduction

Nitrogen oxides (NO and NO_2), which result from automobile exhaust gas and industrial combustion of fossil fuels, have been a major contribution to air pollution.[1] They contribute to photochemical smog, acid rain, ozone depletion and the greenhouse effect. So far, the most efficient technology for the removal of nitrogen oxides from coal-fired power plants has been selective catalytic reduction (SCR) of NO with NH_3.[2] The standard SCR process is based on the following reaction between NH_3 and NO:

$$4NO + 4NH_3 + O_2 \xrightarrow{\text{SCR catalyst}} 4N_2 + 6H_2O \quad (1)$$

Many metal oxide based systems, such as $V_2O_5/WO_3–TiO_2$,[3] $CeO_2/WO_3–TiO_2$,[4] iron titanate[5] and Fe–Ti spinel,[6] have been extensively studied. Among these catalysts, $V_2O_5/WO_3–TiO_2$ has been widely accepted as an industrial catalyst. Although $V_2O_5/WO_3–TiO_2$ has been employed as a commercial SCR catalyst to control the emission of NO_x from coal-fired power plants for several decades, some problems still exist, such as the relatively narrow temperature window of 300–400 °C, the low N_2 selectivity at high temperature, and the toxicity of vanadium pentoxide to the environment.[7] Especially, the price of W resources is now soaring. Therefore, a more cost-effective and more environmentally-friendly SCR catalyst with better N_2 selectivity should be developed.

In this study, WO_3 in $V_2O_5/WO_3–TiO_2$ was substituted by a low cost composition Fe_2O_3 to improve its N_2 selectivity and lower its cost for SCR of NO with NH_3. The support $Fe_2O_3–TiO_2$ was prepared using a co-precipitation method at room temperature, and V_2O_5 was supported on $Fe_2O_3–TiO_2$ by the conventional impregnation method. Then, $V_2O_5/Fe_2O_3–TiO_2$ was characterized using nitrogen physisorption, X-ray diffraction (XRD), X-ray photoelectron spectroscopy (XPS), magnetization and H_2 temperature-programmed reduction (TPR). Subsequently, the SCR performance of $V_2O_5/Fe_2O_3–TiO_2$ was estimated using a packed-bed micro-reactor. At last, the mechanism of the SCR reaction over $V_2O_5/Fe_2O_3–TiO_2$ was studied using *in situ* DRIFTS.

2. Experimental

2.1 Catalyst preparation

The support $Fe_2O_3–TiO_2$ was prepared using a co-precipitation method at room temperature.[8] Suitable amounts of ferrous

[a] *School of Environmental and Biological Engineering, Nanjing University of Science and Technology, Nanjing, 210094, P. R. China*
[b] *State Key Joint Laboratory of Environment Simulation and Pollution Control (SKLESPC), School of Environment, Tsinghua University, Beijing, 100084, P. R. China. E-mail: lijunhua@tsinghua.edu.cn; Fax: +86-10-62771093; Tel: +86-10-62771093*
[c] *School of Environmental Science and Engineering, Shanghai Jiao Tong University, Shanghai, 200240, P. R. China*

sulfate, ferric trichloride, and titanium tetrachloride (Fe^{2+} : Fe^{3+} : Ti^{4+} = 3 : 2 : 1) were dissolved in a HCl solution. This mixture was added to an ammonia solution leading to an instantaneous precipitation. During the reaction, the system was continuously stirred at 800 rpm. The particles were then separated by centrifugation at 4500 rpm for 5 min and washed with distilled water followed by a new centrifugation. After 4 washings, the particles were collected and dried at 105 °C for 12 h.

V_2O_5/Fe_2O_3–TiO_2 catalysts with 1 wt% and 2 wt% V_2O_5 were prepared by the conventional impregnation method using NH_4VO_3 and $H_2C_2O_4{\cdot}2H_2O$ as precursors, and Fe_2O_3–TiO_2 as a support. After the impregnation, excess water was removed in a rotary evaporator at 80 °C. The sample was dried at 105 °C overnight and then calcined at 500 °C for 3 h under air. Meanwhile, Fe_2O_3–TiO_2 was calcined at 500 °C for 3 h under air as a comparison. Furthermore, conventional vanadium-based catalysts (V_2O_5/WO_3–TiO_2) with 1 wt% V_2O_5 and 10 wt% WO_3, and 2 wt% V_2O_5 and 10 wt% WO_3 were prepared by the conventional impregnation method using NH_4VO_3, $(NH_4)_{10}W_{12}O_{41}$ and $H_2C_2O_4{\cdot}2H_2O$ as precursors, and anatase TiO_2 as a support.

2.2 Catalyst characterization

Crystal structure was determined using an X-ray diffractometer (Rigaku, D/max-2200/PC) between 10° and 80° at a step of 7° min^{-1} operating at 30 kV and 30 mA using Cu Kα radiation. BET surface area was determined using a nitrogen adsorption apparatus (Quantachrome, Autosorb-1). The catalyst was outgassed at 200 °C before BET measurement. H_2-TPR was recorded on a chemisorption analyzer (Micromeritics, ChemiSorb 2720 TPx) under a 10% hydrogen–90% nitrogen gas flow (50 cm^3 min^{-1}) at a rate of 10 °C min^{-1}. Saturation magnetization was determined using a vibrating sample magnetometer (VSM, Model JDM-13) at room temperature. X-ray photoelectron spectroscopy (Thermo, ESCALAB 250) was used to determine the Fe 2p, V 2p, Ti 2p and O 1s binding energies with Al Kα (h_v = 1486.6 eV) as the excitation source. The C 1s line at 284.6 eV was taken as a reference for the binding energy calibration.

2.3 Catalytic test

SCR reaction was performed on a fixed-bed quartz tube reactor (6 mm of internal diameter) containing 100–200 mg of the catalyst (40–60 mesh). The typical reactant gas composition was as follows: 500 ppm of NO, 500 ppm of NH_3, 2% of O_2, 10% of H_2O (when used), 200 ppm of SO_2 (when used), and the balance of N_2. The total flow rate was 200 mL min^{-1}, and the gas hourly space velocity (GHSV) varied from about 60 000 to 120 000 cm^3 g^{-1} h^{-1}. The concentrations of NO, NO_2, NH_3 and N_2O were continually monitored by an FTIR spectrometer (Gasmet FTIR DX4000).

As the SCR reaction reached the steady state, the ratios of NO conversion and N_2 selectivity were calculated according to the following equations:

$$\text{NO conversion } \% = \frac{[NO]_{in} - [NO]_{out}}{[NO]_{in}} \times 100\% \qquad (2)$$

$$N_2 \text{ selectivity } \% = 1 - \frac{2[N_2O]_{out} + [NO_2]_{out}}{[NO]_{in} - [NO]_{out} + [NH_3]_{in} - [NH_3]_{out}} \times 100\% \qquad (3)$$

2.4 *In situ* DRIFTS study

In situ DRIFT spectra were recorded on a Fourier transform infrared spectrometer (FTIR, Nicolet NEXUS 870) equipped with a smart collector and an MCT detector cooled by liquid N_2. The diffuse reflectance measurement was carried out *in situ* in a high temperature cell with a ZnSe window. The FTIR spectra were recorded by accumulating 100 scans with a resolution of 4 cm^{-1}.

3. Results

3.1 Characterization

3.1.1 XRD and BET. XRD patterns of synthesized catalysts are shown in Fig. 1. The characteristic peaks of the support Fe_2O_3–TiO_2 corresponded very well to Fe–Ti spinel, and the characteristic peaks corresponding to rutile and anatase did not appear. It indicates that Ti could be introduced into the spinel structure.[9] Furthermore, electron energy loss spectroscopy (EELS), X-ray adsorption near edge structure (XANES) and extended X-ray adsorption fine structure (EXAFS) also demonstrated that Ti could be incorporated into the spinel structure.[10]

After the loading of V_2O_5, the characteristic peaks of V_2O_5/Fe_2O_3–TiO_2 still corresponded very well to Fe–Ti spinel, and additional reflections that would indicate the presence of other crystalline vanadium oxides, such as V_2O_5, VO_2, V_2O_4, V_2O_3 or $FeVO_4$, were not present in the diffraction scan. It indicates that V cations could mainly present as an amorphous phase of VO_x, which was well dispersed on Fe_2O_3–TiO_2.

The BET surface areas of Fe_2O_3–TiO_2, 1% V_2O_5/Fe_2O_3–TiO_2 and 2% V_2O_5/Fe_2O_3–TiO_2 were 81.4, 73.9 and 70.0 m^2 g^{-1}, respectively.

3.1.2 XPS. Surface information of V_2O_5/Fe_2O_3–TiO_2 was analyzed by XPS. XPS spectra over the spectral regions of Fe 2p, Ti 2p, O 1s and V 2p were evaluated (shown in Fig. 2).

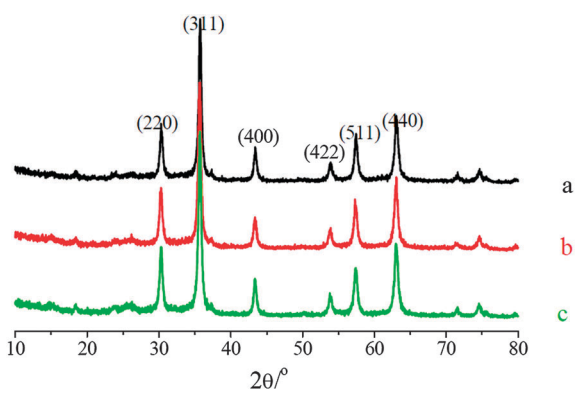

Fig. 1 XRD patterns of: (a) Fe_2O_3–TiO_2; (b) 1% V_2O_5/Fe_2O_3–TiO_2; (c) 2% V_2O_5/Fe_2O_3–TiO_2.

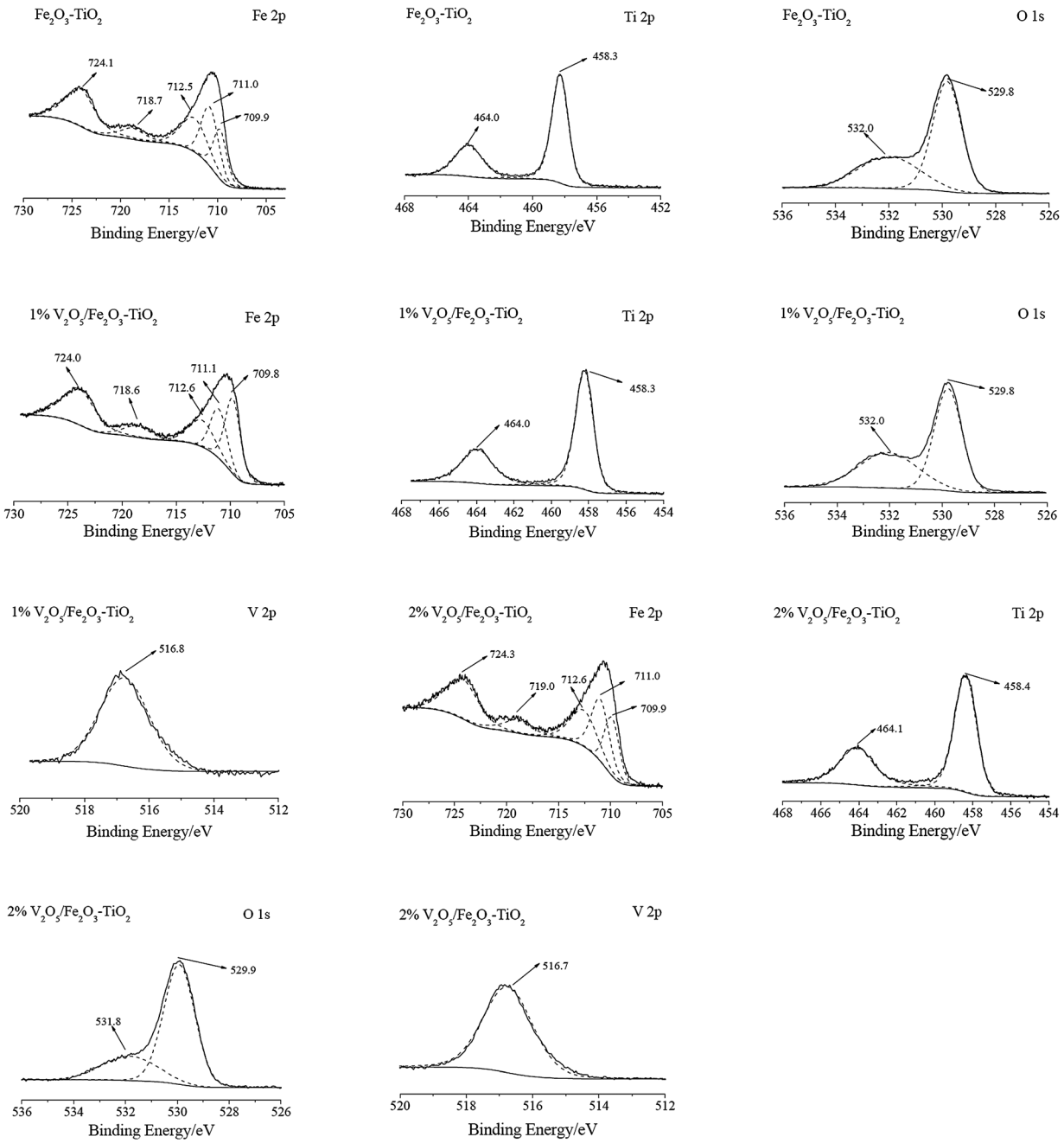

Fig. 2 XPS spectra of V_2O_5/Fe_2O_3–TiO_2 over the spectral regions of Fe 2p, Ti 2p, O 1s and V 2p.

The Fe peaks of Fe_2O_3–TiO_2 were assigned to oxidized Fe species, more likely Fe^{3+} type species. The binding energies centered at about 709.9 eV and 711.0 eV could be assigned to Fe^{3+} in the spinel structure, and the binding energy centered at about 712.5 eV could be ascribed to Fe^{3+} bonded with hydroxyl groups.[11,12] The Ti peaks of Fe_2O_3–TiO_2 were assigned to Ti 2p 1/2 (464.0 eV) and Ti 2p 3/2 (458.3 eV) of Ti^{4+}.[13] The O 1s peaks of Fe_2O_3–TiO_2 mainly centered at about 529.8 eV, as expected for the transition metal oxides. Another oxygen species centered at about 532.0 eV was also observed, which was assigned to –OH.[8]

After the loading of V_2O_5 on Fe_2O_3–TiO_2, no obvious changes happened to XPS spectra of V_2O_5/Fe_2O_3–TiO_2 over the spectral regions of Fe 2p, Ti 2p and O 1s (shown in Fig. 2). The V 2p peak mainly centered at about 516.8 eV, which was assigned to V^{5+}.[14]

The ratios of Fe^{3+}, Ti^{4+}, O^{2-} and V^{5+} on Fe_2O_3–TiO_2, 1% V_2O_5/Fe_2O_3–TiO_2 and 2% V_2O_5/Fe_2O_3–TiO_2 collected from

Table 1 Data of atomic ratios on V_2O_5/Fe_2O_3–TiO_2 collected from XPS/%

	Fe^{3+}	Ti^{4+}	O^{2-}	V^{5+}
Fe_2O_3–TiO_2	28.5	9.5	62.0	—
1% V_2O_5/Fe_2O_3–TiO_2	26.0	9.7	62.6	1.7
2% V_2O_5/Fe_2O_3–TiO_2	22.0	7.9	64.1	6.0

XPS spectra are shown in Table 1. The percentage of V^{5+} on the surfaces of 1% V_2O_5/Fe_2O_3–TiO_2 and 2% V_2O_5/Fe_2O_3–TiO_2 was much more than the content of V^{5+} in 1% V_2O_5/Fe_2O_3–TiO_2 and 2% V_2O_5/Fe_2O_3–TiO_2, respectively. It indicates that V^{5+} could mainly present as an amorphous phase of V_2O_5 on Fe_2O_3–TiO_2. As V_2O_5 was loaded on Fe_2O_3–TiO_2, the percent of Fe^{3+} on V_2O_5/Fe_2O_3–TiO_2 obviously decreased (shown in Table 1). It suggests that the loaded V^{5+} could mainly cover Fe^{3+} on Fe_2O_3–TiO_2.

3.1.3 TPR. H_2-TPR profiles of V_2O_5/Fe_2O_3–TiO_2 are illustrated in Fig. 3. TPR profiles of Fe_2O_3–TiO_2 showed two obvious reduction peaks. The first peak centered at about 442 °C corresponded to the reduction of non-stoichiometric $(Fe_{2.5}Ti_{0.5})_{1-\delta}O_4$ to stoichiometric $Fe_{2.5}Ti_{0.5}O_4$, and the broad peak at higher temperature was attributed to the reduction of $Fe_{2.5}Ti_{0.5}O_4$ to Fe and TiO_2.[8] Our previous study demonstrated that the reduced Fe^{3+} corresponding to the first reduction peak of Fe_2O_3–TiO_2 mainly located in the octahedral site, which resulted from the oxidization of Fe^{2+} in the octahedral site of stoichiometric $Fe_{2.5}Ti_{0.5}O_4$.[8]

After the loading of V_2O_5, a strong displacement of the first reduction peak to low temperature happened in the TPR profiles (shown in Fig. 3). It suggests that the oxidization ability of Fe_2O_3–TiO_2 was gradually enhanced with the increase of V_2O_5 loading.

Because V_2O_5 was loaded on Fe_2O_3–TiO_2, the first step of V_2O_5/Fe_2O_3–TiO_2 reduction was the reduction of V^{5+} on the surface (reaction (4)), and the next step could be the reduction of V^{4+} on the surface (reaction (5)).

$$2{\equiv}V_{Surf}^{5+} + H_2 \rightarrow 2{\equiv}V_{Surf}^{4+} + 2H^+ \quad (4)$$

$$2{\equiv}V_{Surf}^{4+} + H_2 \rightarrow 2{\equiv}V_{Surf}^{3+} + 2H^+ \quad (5)$$

The electrical property of Fe–Ti spinel is similar to that of magnetite, and its band gap is very small.[15] Hence, it has the lower resistivity and its conductivity is almost metallic. As a result, the electron can migrate easily from the bulk to the surface. The redox potential of the reduction of Fe^{3+} by V^{3+} is 0.41 V, so reaction (6) is thermodynamically favorable.[16] Therefore, the formed V^{3+} on the surface could be reoxidized to V^{4+} by the reducible Fe^{3+} in the bulk. Then, the formed V^{4+} on the surface was reduced by gaseous H_2 again. Through the recycle, the reduction of Fe^{3+} in the octahedral site of Fe_2O_3–TiO_2 was promoted. As a result, the first reduction peak of V_2O_5/Fe_2O_3–TiO_2 obviously shifted to low temperature although the amount of V_2O_5 loaded was very small.

$$Fe_{bulk}^{3+} + {\equiv}V_{Surf}^{3+} \rightarrow Fe_{bulk}^{2+} + {\equiv}V_{Surf}^{4+} \quad E^0 = 0.41\ V \quad (6)$$

3.1.4 Magnetization. Vanadium(v) species (*e.g.*, vanadium pentoxide, V_2O_5) are considered particularly toxic with mutagenic effects, respiratory tract toxicity, and possible carcinogenic activity.[17] SCR catalyst can be abraded by the fly ash, and then emits to the fly ash.[18] Therefore, the emission of vanadium based catalyst to the environment during the SCR reaction is a serious concern.

As is well known, the support Fe_2O_3–TiO_2 is a magnetic material.[19] 2% V_2O_5/Fe_2O_3–TiO_2 had the super-paramagnetism with a minimized coercivity and a negligible magnetization hysteresis, and its saturation magnetization was about 43 emu g^{-1} (shown in Fig. 4). The magnetization characteristics ensure that the emission of 2% V_2O_5/Fe_2O_3–TiO_2 to the fly ash during the SCR reaction can be effectively prevented by exposure to an external magnetic field.

3.2 SCR performance

3.2.1 SCR activity and selectivity. 1% V_2O_5/WO_3–TiO_2 showed a moderate SCR activity at 200–250 °C, and an excellent SCR activity at 300–500 °C (shown in Fig. 5a). As the loading of V_2O_5 increased from 1% to 2%, the SCR reaction over V_2O_5/WO_3–TiO_2 was obviously promoted at 150–300 °C. However, NO conversion over 2% V_2O_5/WO_3–TiO_2 gradually decreased with the further increase in reaction temperature from 350 to 500 °C. N_2 selectivity of V_2O_5/WO_3–TiO_2 gradually decreased above 300 °C, and N_2 selectivity of 2% V_2O_5/WO_3–TiO_2 was much worse than that of 1% V_2O_5/WO_3–TiO_2 (shown in Fig. 5b).

Fe_2O_3–TiO_2 showed a moderate SCR activity at 200–300 °C, and an excellent SCR activity at 350–450 °C (shown in Fig. 5a). Meanwhile, little N_2O can be observed during the SCR reaction over Fe_2O_3–TiO_2 (shown in Fig. 5b). The SCR activity of Fe_2O_3–TiO_2 was obviously promoted due to the loading of V_2O_5, and NO conversion over V_2O_5/Fe_2O_3–TiO_2 increased obviously with the increase of V_2O_5 loading (shown in Fig. 5a). Although there was a large amount of V^{5+} on V_2O_5/Fe_2O_3–TiO_2

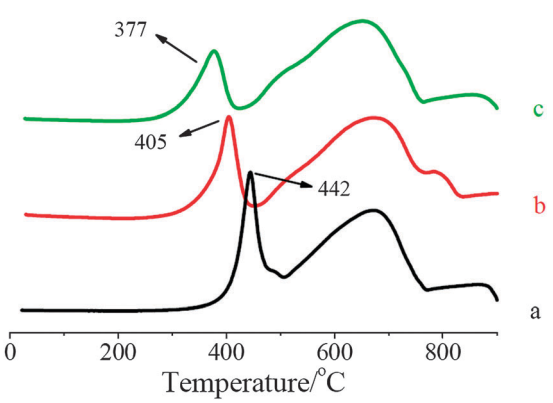

Fig. 3 H_2-TPR profiles of: (a) Fe_2O_3–TiO_2; (b) 1% V_2O_5/Fe_2O_3–TiO_2; (c) 2% V_2O_5/Fe_2O_3–TiO_2.

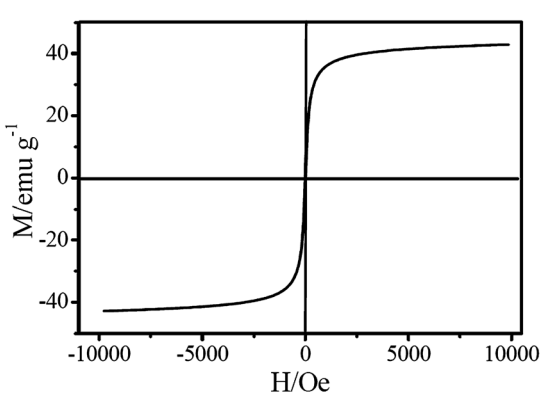

Fig. 4 Magnetization characteristics of 2% V_2O_5/Fe_2O_3–TiO_2.

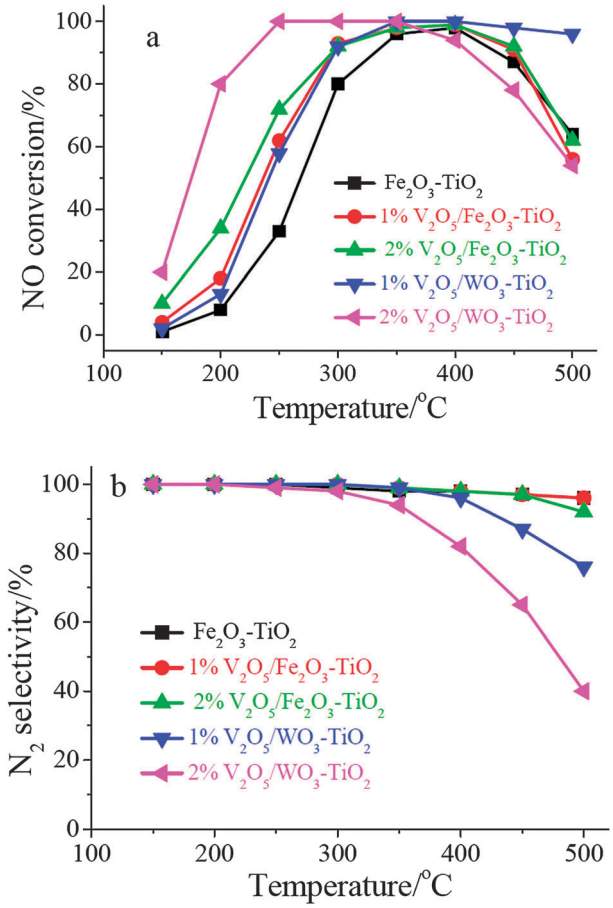

Fig. 5 SCR performance of synthesized catalysts: (a) NO conversion; (b) N_2 selectivity. Reaction conditions: [NO] = [NH_3] = 500 ppm, [O_2] = 2 vol%, catalyst mass = 100 mg, total flow rate = 200 mL min^{-1}, GHSV = 120 000 cm^3 g^{-1} h^{-1}.

(shown in Table 1), V_2O_5/Fe_2O_3–TiO_2 showed an excellent N_2 selectivity. N_2 selectivity of 2% V_2O_5/Fe_2O_3–TiO_2 only slightly decreased to about 90% as the reaction temperature increased to 500 °C, which was much better than those of 1% V_2O_5/WO_3–TiO_2 and 2% V_2O_5/WO_3–TiO_2 (shown in Fig. 5b).

3.2.2 Effect of H_2O and SO_2. Water vapor and SO_2 in the flue gas often lead to the deactivation of the SCR catalyst.[20] Therefore, the effect of 10% of H_2O and 200 ppm of SO_2 on the SCR activity of 2% V_2O_5/Fe_2O_3–TiO_2 was investigated with a 24 h test. As shown in Fig. 6a, the presence of H_2O and SO_2 showed a severe interference with the SCR reaction over 2% V_2O_5/Fe_2O_3–TiO_2 at 150–250 °C. However, the ratio of NO conversion over 2% V_2O_5/Fe_2O_3–TiO_2 in the presence of H_2O and SO_2 can reach above 95% at 300–450 °C, and it did not decrease in the 24 h test. This performance was close to that of 1% V_2O_5/WO_3–TiO_2 (shown in Fig. 6b). It indicates that 2% V_2O_5/Fe_2O_3–TiO_2 had an excellent H_2O and SO_2 durability in the temperature range of the SCR unit of the coal-fired power plant.

3.3 *In situ* DRIFTS study

3.3.1 *In situ* DRIFTS study on V_2O_5/WO_3–TiO_2. After 2% V_2O_5/WO_3–TiO_2 was treated with NH_3/N_2 at 250 °C, the

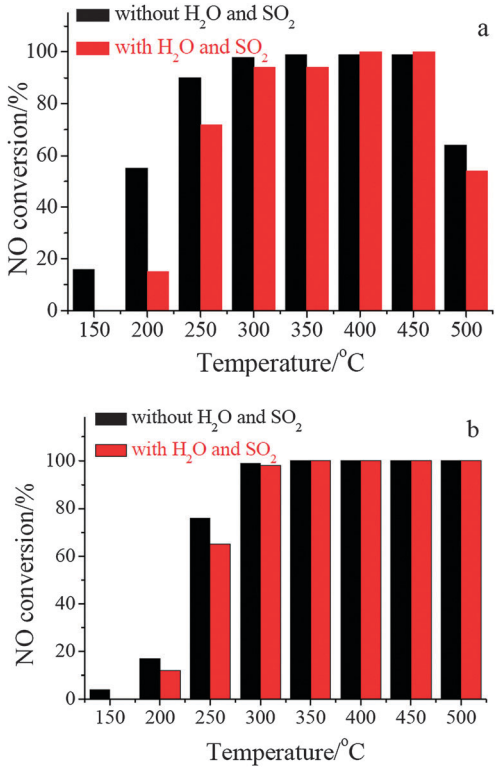

Fig. 6 Effect of 10% of H_2O and 200 ppm of SO_2 on the SCR reaction over: (a) 2% V_2O_5/Fe_2O_3–TiO_2; (b) 1% V_2O_5/WO_3–TiO_2. Reaction condition: [NO] = [NH_3] = 500 ppm, [O_2] = 2 vol%, catalyst mass = 200 mg, total flow rate = 200 mL min^{-1}, GHSV = 60 000 cm^3 g^{-1} h^{-1}.

characteristic vibrations mainly centered at 1425 and 1245 cm^{-1} (shown in Fig. 7a). The band at 1425 cm^{-1} was assigned to ionic NH_4^+ bound to the Brønsted acid sites, and the band at 1245 cm^{-1} was attributed to coordinated NH_3 bound to the Lewis acid sites.[21] After NO + O_2/N_2 passed over NH_3 pretreated 2% V_2O_5/WO_3–TiO_2 at 250 °C, both ionic NH_4^+ and coordinated NH_3 diminished (shown in Fig. 7a). Meanwhile, adsorbed H_2O, which is a product of the SCR reaction, can be clearly observed at 1620 cm^{-1}.[22] They both suggest that adsorbed ammonia species on 2% V_2O_5/WO_3–TiO_2 can react with NO.

After 2% V_2O_5/WO_3–TiO_2 was treated with NO + O_2/N_2 at 250 °C, the bands corresponding to adsorbed NO_x species were hardly observed (shown in Fig. 7b). It suggests that gaseous NO can hardly adsorb on 2% V_2O_5/WO_3–TiO_2 to form adsorbed NO_x. After NH_3/N_2 passed over NO + O_2 pretreated 2% V_2O_5/WO_3–TiO_2, its surface was mainly covered by ionic NH_4^+ bound to the Brønsted acid sites and coordinated NH_3 bound to the Lewis acid sites. Furthermore, adsorbed H_2O, which is a product of the SCR reaction, can hardly be detected at about 1620 cm^{-1}. It suggests that the reaction between ammonia and adsorbed nitrogen oxide species cannot happen on 2% V_2O_5/WO_3–TiO_2. Therefore, the SCR reaction over V_2O_5/WO_3–TiO_2 mainly followed the Eley–Rideal mechanism.

3.3.2 *In situ* DRIFTS study on Fe_2O_3–TiO_2. Fe_2O_3–TiO_2 was mainly covered by ionic NH_4^+ bound to the Brønsted acid sites (1430 cm^{-1}) and coordinated NH_3 bound to the Lewis acid sites (1221 and 1606 cm^{-1}) after the treatment of

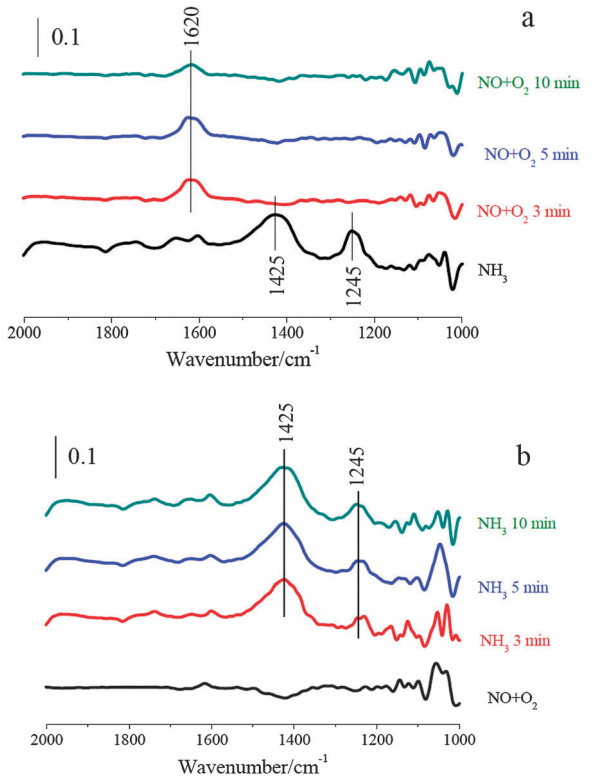

Fig. 7 (a) *In situ* DRIFT spectra taken at 250 °C upon passing NO + O_2 over NH_3 presorbed 2% $V_2O_5/WO_3–TiO_2$; (b) *in situ* DRIFT spectra taken at 250 °C upon passing NH_3 over NO + O_2 presorbed 2% $V_2O_5/WO_3–TiO_2$.

NH_3/N_2 at 250 °C (shown in Fig. 8a). After NO + O_2/N_2 passed over NH_3 pretreated $Fe_2O_3–TiO_2$ at 250 °C, both ionic NH_4^+ and coordinated NH_3 diminished (shown in Fig. 8a). It suggests that adsorbed ammonia species on $Fe_2O_3–TiO_2$ can react with NO. Meanwhile, three new vibrations at 1614, 1576 and 1551 cm^{-1} appeared, which were assigned to monodentate nitrite and monodentate nitrate respectively.[22]

After the adsorption of NO + O_2 at 250 °C, $Fe_2O_3–TiO_2$ was mainly covered by monodentate nitrite and monodentate nitrate (1614, 1576, 1551 and 1371 cm^{-1}). After NH_3/N_2 passed over NO + O_2 pretreated $Fe_2O_3–TiO_2$ at 250 °C, the bands corresponding to adsorbed NO_x species disappeared. Meanwhile, the bands at 1606, 1430 and 1221 cm^{-1} corresponding to adsorbed ammonia species appeared. It suggests that adsorbed NO_x could take part in the SCR reaction over $Fe_2O_3–TiO_2$.

At last, the IR spectra during the SCR reaction (*i.e.* NH_3 and NO + O_2 were simultaneously introduced) over $Fe_2O_3–TiO_2$ at 250 °C were recorded. As shown in Fig. 8c, $Fe_2O_3–TiO_2$ was mainly covered by ionic NH_4^+ bound to the Brønsted acid sites (1430 cm^{-1}) and coordinated NH_3 bound to the Lewis acid sites (1221 and 1606 cm^{-1}), and the characteristic vibrations corresponding to adsorbed NO_x species were hardly observed. It suggests that the adsorption of NO + O_2 on $Fe_2O_3–TiO_2$ could not happen in the presence of NH_3. There is general agreement that the SCR reaction starts with the adsorption of NH_3, which is very strong compared to the adsorption of NO + O_2 and the reaction products.[23]

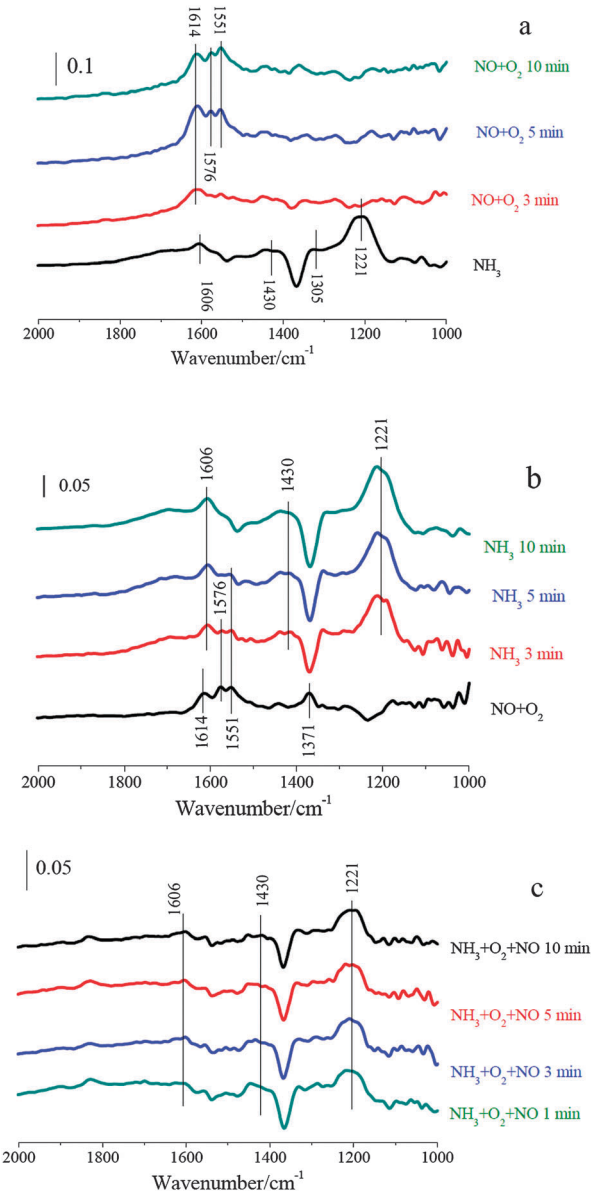

Fig. 8 (a) *In situ* DRIFT spectra taken at 250 °C upon passing NO + O_2 over NH_3 presorbed 2% $Fe_2O_3–TiO_2$; (b) *in situ* DRIFT spectra taken at 250 °C upon passing NH_3 over NO + O_2 presorbed $Fe_2O_3–TiO_2$; (c) *in situ* DRIFT spectra taken at 250 °C upon passing NO + O_2 + NH_3 over 2% $Fe_2O_3–TiO_2$.

Therefore, The SCR reaction over $Fe_2O_3–TiO_2$ mainly followed the Eley–Rideal mechanism.

3.3.3 *In situ* DRIFTS study on $V_2O_5/Fe_2O_3–TiO_2$. After 2% $V_2O_5/Fe_2O_3–TiO_2$ was treated with NH_3/N_2 at 250 °C, $V_2O_5/Fe_2O_3–TiO_2$ was mainly covered by ionic NH_4^+ bound to the Brønsted acid sites (1430 cm^{-1}) and coordinated NH_3 bound to the Lewis acid sites (1221 and 1606 cm^{-1}). The characteristic vibration corresponding to NH_3 adsorbed on $V_2O_5/Fe_2O_3–TiO_2$ was the same as that on $Fe_2O_3–TiO_2$ (shown in Fig. 8a and 9a), and it was quite different from that on $V_2O_5/WO_3–TiO_2$ (shown in Fig. 7a and 9a). It suggests that the acid sites (*i.e.* Brønsted acid sites and Lewis acid sites) on $V_2O_5/Fe_2O_3–TiO_2$ mainly resulted from the support $Fe_2O_3–TiO_2$,

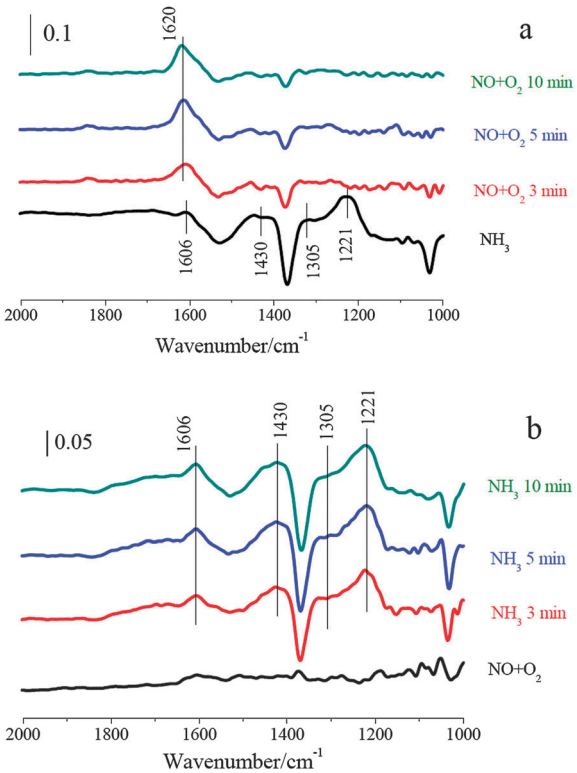

Fig. 9 (a) *in situ* DRIFT spectra taken at 250 °C upon passing NO + O_2 over NH_3 presorbed 2% V_2O_5/Fe_2O_3–TiO_2; (b) *in situ* DRIFT spectra taken at 250 °C upon passing NH_3 over NO + O_2 presorbed 2% V_2O_5/Fe_2O_3–TiO_2.

and the effect of V_2O_5 loading on the acid sites can be approximately neglected. After NO + O_2/N_2 passed over NH_3 pretreated 2% V_2O_5/Fe_2O_3–TiO_2 at 250 °C, both ionic NH_4^+ and coordinated NH_3 diminished (shown in Fig. 9a). Meanwhile, adsorbed H_2O, which is a product of the SCR reaction, was clearly observed at 1620 cm^{-1}.[22] They both suggest that adsorbed ammonia species on 2% V_2O_5/Fe_2O_3–TiO_2 can react with NO.

After 2% V_2O_5/Fe_2O_3–TiO_2 was treated with NO + O_2/N_2 at 250 °C, the bands corresponding to adsorbed nitrite and nitrate cannot be observed (shown in Fig. 9b). It indicates that the active sites on Fe_2O_3–TiO_2 for the adsorption of gaseous NO were covered by the loaded V_2O_5. Hence, the adsorption of gaseous NO on Fe_2O_3–TiO_2 was restrained due to the loading of V_2O_5. After NH_3/N_2 passed over NO + O_2 pretreated 2% V_2O_5/Fe_2O_3–TiO_2, its surface was mainly covered by ionic NH_4^+ bound to the Brønsted acid sites and coordinated NH_3 bound to the Lewis acid sites. Furthermore, adsorbed H_2O, which is a product of the SCR reaction, can hardly be detected at about 1620 cm^{-1}. It suggests that the reaction between adsorbed nitrogen oxide species and ammonia cannot happen on 2% V_2O_5/Fe_2O_3–TiO_2. Therefore, the SCR reaction over V_2O_5/Fe_2O_3–TiO_2 mainly followed the Eley–Rideal mechanism.

4. Discussion

The SCR reaction over Fe_2O_3–TiO_2 can be approximately described as follows:[6]

$$NH_{3(g)} \rightleftharpoons NH_{3(ad)} \quad (7)$$

$$NH_{3(ad)} + \equiv Fe_{Surf}^{3+} \rightarrow -NH_2 + \equiv Fe_{Surf}^{2+} + H^+ \quad (8)$$

$$-NH_2 + NO_{(g)} \rightarrow N_2 + H_2O \quad (9)$$

$$\equiv Fe_{Surf}^{2+} + \tfrac{1}{4}O_2 \rightarrow \equiv Fe_{Surf}^{3+} + \tfrac{1}{2}\equiv O \quad (10)$$

Meanwhile, the SCR reaction over V_2O_5/WO_3–TiO_2 can be approximately described as follows:[24]

$$NH_{3(g)} \rightleftharpoons NH_{3(ad)} \quad (7)$$

$$NH_{3(ad)} + \equiv V_{Surf}^{5+} \rightarrow -NH_2 + \equiv V_{Surf}^{4+} + H^+ \quad (11)$$

$$-NH_2 + NO_{(g)} \rightarrow N_2 + H_2O \quad (9)$$

$$\equiv V_{Surf}^{4+} + \tfrac{1}{4}O_2 \rightarrow \equiv V_{Surf}^{5+} + \tfrac{1}{2}\equiv O \quad (12)$$

Reaction (7) was the adsorption of gaseous ammonia on the acid sites (*i.e.* Brønsted acid sites and Lewis acid sites) to form adsorbed ammonia species including ionic NH_4^+ and coordinated NH_3. Reactions (8) and (11) were the activation of adsorbed ammonia species by Fe^{3+} and V^{5+} on the surface to form amide species ($-NH_2$), respectively. Then, gaseous NO was reduced by $-NH_2$ on the surface to form N_2 and H_2O (reaction (9)). Reactions (10) and (12) were the reoxidization of formed Fe^{2+} and V^{4+}, respectively. Therefore, the SCR reaction over V_2O_5/Fe_2O_3–TiO_2 can be approximately described using reactions (7–12) and both V^{5+} and Fe^{3+} could be the active components for the activation of adsorbed NH_3.

In situ DRIFTS study demonstrated that the acid sites on V_2O_5/Fe_2O_3–TiO_2 mainly resulted from Fe_2O_3–TiO_2, and gaseous NH_3 mainly adsorbed onto Fe_2O_3–TiO_2. Therefore, the adsorbed NH_3 on V_2O_5/Fe_2O_3–TiO_2 preferred to be activated by Fe^{3+} rather than V^{5+} on V_2O_5/Fe_2O_3–TiO_2. Moreover, the oxidization of Fe^{2+} by V^{5+} is thermodynamically favorable because the redox potential of reaction (13) is 0.23 V. Therefore, the regeneration of Fe^{3+} on Fe_2O_3–TiO_2 could be accelerated due to the rapid electron transfer between V^{5+} and Fe^{2+} on V_2O_5/Fe_2O_3–TiO_2.[16]

$$\equiv Fe_{Surf}^{2+} + \equiv V_{Surf}^{5+} \rightarrow \equiv Fe_{Surf}^{3+} + \equiv V_{Surf}^{4+} \quad E^0 = 0.23\ V \quad (13)$$

At 150–300 °C, a large amount of NO cannot be reduced over Fe_2O_3–TiO_2 (shown in Fig. 5a). It indicates that adsorbed NH_3 cannot be completely activated by Fe^{3+} on Fe_2O_3–TiO_2 at 150–300 °C. The loading of V_2O_5 accelerated the regeneration of Fe^{3+} on Fe_2O_3–TiO_2 through reaction (13), which promoted the activation of adsorbed NH_3 by Fe^{3+} on Fe_2O_3–TiO_2. Furthermore, NH_3 adsorbed on V_2O_5/Fe_2O_3–TiO_2, which was not activated by Fe^{3+}, could then be activated by V^{5+} on the surface. As a result, the SCR activity of Fe_2O_3–TiO_2 improved due to the loading of V_2O_5. However, the oxidization ability of Fe^{3+} is much less than that of V^{5+}, so the activation of NH_3 by Fe^{3+} was much slower than that by V^{5+}. As a result, the SCR activity of 2% V_2O_5/Fe_2O_3–TiO_2 was much less than that of 2% V_2O_5/WO_3–TiO_2 at 150–300 °C.

Some adsorbed NH_3 could be over-oxidized by V^{5+} cations on the surface to form −NH or −N above 300 °C. Then, −NH or −N reacted with gaseous NO to form N_2O.[25] Therefore, N_2 selectivity of V_2O_5/WO_3–TiO_2 obviously decreased above 300 °C (shown in Fig. 5b). If a large amount of NH_3 adsorbed on V_2O_5/Fe_2O_3–TiO_2 was activated by V^{5+} above 300 °C,

some N_2O should form. However, little N_2O formed over $V_2O_5/Fe_2O_3–TiO_2$ (shown in Fig. 5b). It suggests that NH_3 adsorbed on $V_2O_5/Fe_2O_3–TiO_2$ was mainly activated by Fe^{3+} above 300 °C.

NO conversion over $Fe_2O_3–TiO_2$ obviously increased as the reaction temperature increased from 200 to 400 °C (shown in Fig. 5a). It suggests that the activation of adsorbed NH_3 by Fe^{3+} on $Fe_2O_3–TiO_2$ (reaction (8)) was obviously promoted with the increase in reaction temperature. As shown in Fig. 5a, more than 80% of gaseous NO can be reduced over $Fe_2O_3–TiO_2$ at 350–450 °C. It suggests that most of the adsorbed NH_3 could be activated by Fe^{3+} on $V_2O_5/Fe_2O_3–TiO_2$ even if V^{5+} did not take part in the activation of adsorbed NH_3. Because gaseous NH_3 mainly adsorbed on $Fe_2O_3–TiO_2$, the adsorbed NH_3 preferred to be activated by Fe^{3+} rather than by V^{5+} on $V_2O_5/Fe_2O_3–TiO_2$. Meanwhile, the ratios of Fe^{3+} to V^{5+} on 1% and 2% $V_2O_5/Fe_2O_3–TiO_2$ were 15.3 and 3.7, respectively. Therefore, reaction (8) predominated over the activation of adsorbed NH_3 during the SCR reaction over $V_2O_5/Fe_2O_3–TiO_2$ at 350–500 °C. As a result, $V_2O_5/Fe_2O_3–TiO_2$ showed an excellent N_2 selectivity at 350–500 °C. Because the regeneration of Fe^{3+} on $Fe_2O_3–TiO_2$ was accelerated due to the loading of V_2O_5, the SCR activity of $V_2O_5/Fe_2O_3–TiO_2$ was generally better than that of $Fe_2O_3–TiO_2$ at 350–450 °C.

5. Conclusion

2% $V_2O_5/Fe_2O_3–TiO_2$ showed excellent SCR activity, N_2 selectivity and H_2O/SO_2 durability at 300–450 °C. Meanwhile, the emission of 2% $V_2O_5/Fe_2O_3–TiO_2$ to the fly ash can be prevented by an external magnetic field due to its inherent magnetization. Therefore, 2% $V_2O_5/Fe_2O_3–TiO_2$ could be a promising low-cost SCR catalyst to control of the emission of NO.

Acknowledgements

This study was financially supported by the National Natural Science Fund of China (Grant Nos. 51078203 and 21207067), the National High-Tech Research and Development (863) Program of China (Grant Nos. 2010AA065002 and 2012AA062506).

Notes and references

1 G. S. Qi, R. T. Yang and R. Chang, *Appl. Catal., B*, 2004, **51**, 93–106.
2 Z. Wu, B. Q. Jiang and Y. Liu, *Appl. Catal., B*, 2008, **79**, 347–355.
3 N. Y. Topsoe, *Science*, 1994, **265**, 1217–1219.
4 L. Chen, J. H. Li and M. F. Ge, *Environ. Sci. Technol.*, 2010, **44**, 9590–9596.
5 F. D. Liu, H. He, C. B. Zhang, Z. C. Feng, L. R. Zheng, Y. N. Xie and T. D. Hu, *Appl. Catal., B*, 2010, **96**, 408–420.
6 S. J. Yang, J. H. Li, C. Z. Wang, J. H. Chen, L. Ma, H. Z. Chang, L. Chen, Y. Peng and N. Q. Yan, *Appl. Catal., B*, 2012, **117**, 73–80.
7 L. Chen, J. H. Li and M. F. Ge, *J. Phys. Chem. C*, 2009, **113**, 21177–21184.
8 S. Yang, Y. Guo, N. Yan, D. Wu, H. He, Z. Qu, C. Yang, Q. Zhou and J. Jia, *ACS Appl. Mater. Interfaces*, 2011, **3**, 209–217.
9 S. Yang, H. He, D. Wu, D. Chen, X. Liang, Z. Qin, M. Fan, J. Zhu and P. Yuan, *Appl. Catal., B*, 2009, **89**, 527–535.
10 P. Perriat, E. Fries, N. Millot and B. Domenichini, *Solid State Ionics*, 1999, **117**, 175–184.
11 S. Yang, Y. Guo, N. Yan, Z. Qu, J. Xie, C. Yang and J. Jia, *J. Hazard. Mater.*, 2011, **186**, 508–515.
12 S. J. Yang, Y. F. Guo, N. Q. Yan, D. Q. Wu, H. P. He, Z. Qu and J. P. Jia, *Ind. Eng. Chem. Res.*, 2011, **50**, 9650–9656.
13 S. Yang, Y. Guo, N. Yan, D. Wu, H. He, J. Xie, Z. Qu and J. Jia, *Appl. Catal., B*, 2011, **101**, 698–708.
14 S. Yang, Y. Guo, N. Yan, D. Wu, H. He, J. Xie, Z. Qu, C. Yang and J. Jia, *Chem. Commun.*, 2010, **46**, 8377–8379.
15 N. Guigue-Millot, Y. Champion, M. J. Hytch, F. Bernard, S. Begin-Colin and P. Perriat, *J. Phys. Chem. B*, 2001, **105**, 7125–7132.
16 X. L. Liang, S. Y. Zhu, Y. H. Zhong, J. X. Zhu, P. Yuan, H. P. He and J. Zhang, *Appl. Catal., B*, 2010, **97**, 151–159.
17 M. M. Shafer, B. M. Toner, J. T. Oyerdier, J. J. Schauer, S. C. Fakra, S. H. Hu, J. D. Herner and A. Ayala, *Environ. Sci. Technol.*, 2012, **46**, 189–195.
18 S. Yang, C. Wang, J. Chen, Y. Peng, L. Ma, H. Chang, H. Chang, C. Liu, J. Li and N. Yan, *Catal. Sci. Technol.*, 2012, **2**, 915–917.
19 S. J. Yang, H. P. He, D. Q. Wu, D. Chen, Y. H. Ma, X. L. Li, J. X. Zhu and P. Yuan, *Ind. Eng. Chem. Res.*, 2009, **48**, 9915–9921.
20 F. D. Liu, K. Asakura, H. He, W. P. Shan, X. Y. Shi and C. B. Zhang, *Appl. Catal., B*, 2010, **103**, 369–377.
21 G. S. Qi and R. T. Yang, *J. Phys. Chem. B*, 2004, **108**, 15738–15747.
22 S. Yang, C. Wang, J. Li, N. Yan, L. Ma and H. Chang, *Appl. Catal., B*, 2011, **110**, 71–80.
23 W. S. Kijlstra, D. S. Brands, H. I. Smit, E. K. Poels and A. Bliek, *J. Catal.*, 1997, **171**, 219–230.
24 G. Busca, L. Lietti, G. Ramis and F. Berti, *Appl. Catal., B*, 1998, **18**, 1–36.
25 X. F. Tang, J. H. Li, L. A. Sun and J. M. Hao, *Appl. Catal., B*, 2010, **99**, 156–162.